LA-UR 94-0385

Conf-9310271--1

Los Alamos National Laboratory is operated by the University of California for the United States Department of Energy under contract W-7405-ENG-36.

TITLE: MASS MODEL FOR UNSTABLE NUCLEI

AUTHOR(S): Peter Möller
J. Rayford Nix

SUBMITTED TO: Presented at the Conference on Simulation Study on Hadronic Many-Body System, JAERI, Tokai-mura, Ibaraki, Japan, October 18-20, 1993

DISCLAIMER

Los Alamos National Laboratory
Los Alamos, New Mexico 87545

FORM NO 836 R4
ST NO 2629 5/81

Mass model for unstable nuclei

Peter Möller†and J Rayford Nix‡

† Japan Atomic Research Institute, Tokai, Naka-gun, Ibaraki, 319-11 Japan

‡ Theoretical Division, Los Alamos National Laboratory, Los Alamos, NM 87545, USA

Abstract. We present some essential features of a macroscopic-microscopic nuclear-structure model, with special emphasis on the results of a recent global calculation of nuclear masses. We discuss what should be some minimal requirements of a nuclear mass model and study how the macroscopic-microscopic method and other nuclear mass models fullfil such basic requirements. We study in particular the reliability of nuclear mass models in regions of nuclei that were not considered in the determination of the model parameters.

1. Introduction

An understanding of the reliability of nuclear-structure models far from stability is of great importanance for the design of experiments leading to reaction products far from stability, for astrophysical applications, and for many other applications. Here we discuss several nuclear-structure models but focus most of our presentation on results obtained in the macroscopic-microscopic method applied to nuclear masses. In contrast to many other mass models the macroscopic-microscopic method does not diverge when applied to nuclei outside the region where its parameters were adjusted It can also describe such diverse properties as nuclear energy levels, ground-state masses and shapes, β-decay properties and fission-barrier heights.

In the macroscopic-microscopic method, the energy of a nucleus is calculated as the sum of two contributions. The macroscopic energy gives the smooth trends, and the microscopic correction gives the fluctuations about the smooth trends. The former contribution can be determined from a liquid-drop model, droplet model, Thomas-Fermi model, or similar macroscopic model. In *nuclear mass* calculations two radically different approaches have usually been used to determine the latter contribution. In one approach the microscopic correction is determined from calculated single-particle levels by use of Strutinsky's method. In the other approach an expression for the microscopic correction is postulated, with the parameters of this expression adjusted to reproduce experimental data. In this latter approach different parameters are required for each deformed region. Other nuclear mass models are based on other concepts, such as the nuclear shell-model and the Garvey-Kelson mass relations. We discuss here the relative merits of the different models and make detailed comparisons.

Like any physical theory, a theory of nuclear masses should fulfill certain standard requirements. For example, it should be able to describe several related phenomena in terms of *a few* simple assumptions, have predictive power, be able to provide new physical insight,

and be capable of being disproved. It is reasonable to require that a theory of nuclear masses predict the energy of any minimum that occurs when the shape of the nucleus is varied, irrespective of whether it is the lowest, ground-state minimum or a shape-isomeric minimum. It is also natural to require that it predict the next magic proton and neutron numbers beyond ^{208}Pb. If this is not possible one cannot have confidence that it can correctly predict effects related to gaps in regions far from β-stability. To study the reliability of different mass models far from β-stability, we investigate the results of various approaches when applied to new regions of nuclei that were not considered when the theories were formulated or its parameters determined.

2. Macroscopic-microscopic model

Most models that have been used for calculating a large number of nuclear-structure properties for extended regions of nuclei are based on the macroscopic-microscopic method. There are several possible choices of macroscopic models and also several possible choices of single-particle models. For each of these models several reasonable parameter sets may exist. Thus, over the years hundreds of different macroscopic-microscopic calculations have been published. Although many of these calculations are based on very similar models, there usually exist significant differences between their detailed predictions. It is our experience that to fully understand nuclear structure in terms of an underlying model, one has to develop the model in a careful and consistent manner, and avoid switching back and forth between various formulations of the model with no clear idea of which is the preferred formulation. We illustrate this principle with a couple of examples from our own work over the years. In particular, we illustrate how improvements of the calculations lead to the discovery of new physical effects.

2.1. Macroscopic models

In most early applications of the macroscopic-microscopic method [1–5]) the macroscopic model of choice has been the standard liquid-drop model [6,7]). However, later several extensions to the liquid-drop model have been developed.

The droplet model [8–10]) expands the energy to one higher order in $A^{-1/3}$ and relative neutron excess $I = (N - Z)/(N + Z)$, which allows for the inclusion of compressibility effects and a neutron skin. However, many applications of the droplet model [10,11]) to the calculation of nuclear masses far from stability indicated that the nuclear mass surface was too soft. As a consequence, the neutron drip line was predicted to be about 20 neutrons further from stability than indicated by astrophysical evidence.

In a different approach, the liquid-drop model was generalized to the finite-range liquid-drop model [12,13]) by modification of the surface-energy term to account for the finite range of the nuclear force. This reduces the surface energy for shapes with a pronounced neck or for configurations of nearly touching nuclei in heavy-ion collisions. Thus, fission-barrier heights for nuclei in the vicinity of $A = 100$ are calculated to be about 40 MeV, in good agreement with measured values. In contrast, the liquid-drop model and droplet model both give substantially higher barrier heights for nuclei in this region. For the interaction barrier in heavy-ion collisions the finite-range liquid-drop model gives results that are similar to those obtained by use of the proximity-force model [14]), but is more general.

The combination of this macroscopic term with the folded-Yukawa single-particle model we designate the finite-range liquid-drop model (FRLDM) [15]), which abbreviation is also used for the macroscopic model only. In an application [16,17]) of the first formulation of this model to the calculation of nuclear masses and fission barriers throughout the periodic system the FRLDM gave excellent results. However, the macroscopic part in this formulation does not

describe such features as nuclear compressibility and corresponding variations in the proton and neutron radii.

The droplet model[8-10], an extension of the original liquid-drop model[6], does describe such features. The well-known deficiencies of its original formulation led Myers to suggest that the surface-energy terms of the droplet model be generalized to account for the finite range of the nuclear force. During this work it also became apparent that the description of nuclear compressibility needed improvement. The new macroscopic model[18,19] that resulted, the finite-range droplet model, is labeled by FRDM, which also denotes its combination with the folded-Yukawa single-particle model.

2.2. Microscopic models

In the more fundamental version of the macroscopic-microscopic approach the microscopic correction is determined from calculated single-particle levels by use of Strutinsky's method[1,2]. Reviews of early work may be found in refs.[4,20,21]. Commonly used potentials are the folded-Yukawa[5,16,22], Woods-Saxon[23], modified-oscillator[3] and two-center oscillator[24] single-particle potentials. The pure single-particle models alone are inappropriate for calculating total potential energies or transition probabilities. In potential-energy calculations it is necessary to include residual pairing interactions treated in either the BCS[20,25-28] or Lipkin-Nogami[29-33] approximation. In calculations of transition rates additional residual interactions, specific to the transition operator, must also be included. In studies of Gamow-Teller β-decay a residual Gamow-Teller interaction is treated in the quasi-particle random-phase (QRPA) approximation[34-38].

3. Calculated nuclear-structure properties

As a first step in studying nuclear decay properties it is natural to determine the nuclear ground-state shape. Once the ground-state deformation parameters are known, the nuclear ground-state mass and nuclear wave functions may be calculated. Matrix elements giving β-decay transition rates and many other quantities of interest can also be determined. Studies of fission properties require calculating the nuclear potential-energy surface for shapes relevant to the fission process. In addition, the inertia tensor must be determined.

3.1. Nuclear potential energy of deformation

To determine the nuclear ground-state shape one must minimize the nuclear potential energy with respect to the shape of the nuclear surface. This cannot be done analytically so in practice one calculates the potential energy for a set of deformation parameters and determines the minimum numerically from the energy in the calculated grid points. A common method is to draw an energy contour diagram based on the energy in the calculated grid points and locate the minimum in the contour diagram.

In fig. 1 we show a typical result of a calculation of the nuclear potential energy of deformation for the nucleus ^{240}Pu. The calculation was carried out for a two-dimensional grid in the Nilsson perturbed-spheroid parameterization in 378 gridpoints by using 27 equidistant values of ϵ_2 ($\epsilon_2 = -0.30, 0.25, \ldots, 1.0$) and 14 equidistant values of ϵ_4' ($\epsilon_4' = -0.24, -0.20, \ldots, 0.28$), where $\epsilon_4' = \epsilon_4$ if $\epsilon_2 \leq 0.25$ and $\epsilon_4' = \epsilon_4 + (\epsilon_2 - 0.25)/5.0$ if $\epsilon_2 \geq 0.25$ Since the appearance of a contour diagram is strongly dependent on the particular variables in terms of which it is displayed it is normally best to avoid displaying the calculated results in terms of the parameters of the actual parameterization. Instead it is best displayed in terms of parameters that characterize the shape in a more general way. One possible choice would be to display the

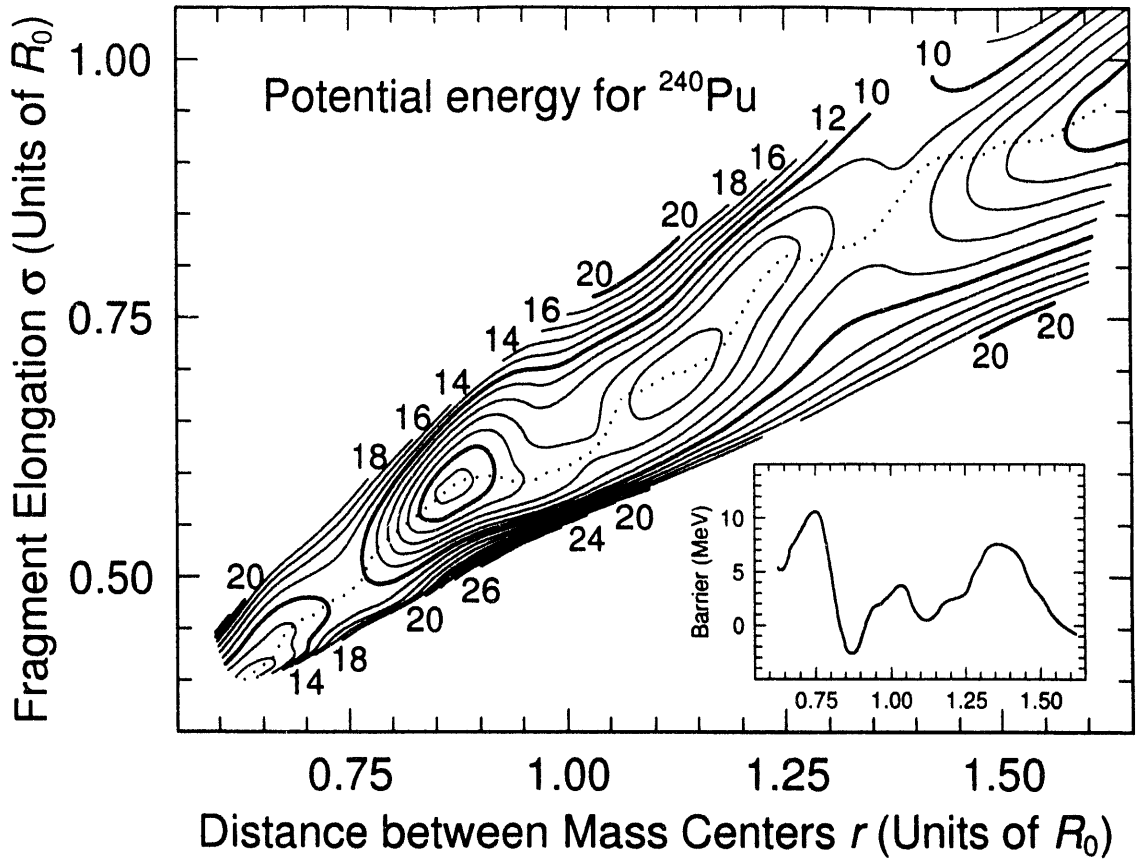

Figure 1. Calculated potential-energy surface for ^{240}Pu for symmetric deformations. The insert corresponds to the potential energy along the dotted line.

contour diagram in terms of the multipole moments of the shape. However, then the inertia of two separated fragments would not be constant, which would complicate the interpretation of fission potential-energy surfaces. Therefore we have often chosen to display calculated potential-energy surfaces in terms of the two moments r and σ [39,40]), where r is the distance between the centers of mass of the two halves of the system and σ is the sum of the root-mean-square extensions along the symmetry axis of the mass of each half of the system about its center of mass.

Figure 1 is based on a sufficiently large grid to show almost the entire barrier that a nucleus undergoing symmetric fission would have to penetrate. Fission and barrier penetration are multidimensional concepts, but to obtain a one-dimensional picture one often plots the energy along a path through the minima and saddle points in the multidimensional space versus r. In the insert we see such a one-dimensional fission barrier corresponding to the dotted path in the two-dimensional contour diagram. The contour diagram illustrates that there are several minima in the potential-energy surface. The minimum at $r/R_0 = 1.12$ is the fission isomeric state. The deepest minimum at $r/R_0 = 0.87$ is the nuclear ground state. The contours are plotted relative to the spherical macroscopic energy. A third minimum in the lower left corner represents an oblate local minimum.

3.2. Inadequacy of models without deformation

Oblate minima can sometimes become lower than the prolate minima. In our calculations of ground-state shapes of 8979 nuclei we find that for 771 nuclei $\epsilon_2 \leq -0.10$ and for 5558 nuclei

$\epsilon_2 \geq 0.10$. The occurrence of oblate minima is the reason we feel that models that do not incorporate deformation can never properly describe nuclear masses. To illustrate this, let us for simplicity discuss the case of a multiparameter mass model of a type that contains an expression whose parameters are adjusted by minimizing the rms deviation between calculated and measured masses. Suppose further that in some region of the nuclear chart nuclei have both oblate and prolate minima but that the oblate minima for all known masses are about 1 MeV higher than the prolate minima. The nuclear mass "model" describes the nuclear masses corresponding to these prolate minima well. Now we assume that new nuclei are discovered in this region, and that the oblate minima becomes lower than the prolate minima by say 2 MeV, because for oblate shapes a large energy gap appears in the level diagrams at the appropriate nucleon numbers. In this situation the multiparameter model that does not account for deformation would predict a mass corresponding to the prolate minimum, and be in error by about 2 MeV.

3.3. Nuclear masses

Our own work on nuclear mass models has now resulted in a preferred formulation based on the folded-Yukawa single-particle potential and the finite-range droplet model. It will be completely specified in a forthcoming contribution to Atomic Data and Nuclear Data Tables [29]). This model has its origin in a 1981 nuclear mass model [16]) which utilized the folded-Yukawa single-particle potential developed in 1972 [5]). One important feature of the 1981 calculation was the use of an improved choice [22]) for the spin-orbit and diffuseness parameters of the potential. Another was the use of the finite-range liquid-drop model as the microscopic model. The FRLDM is of importance both for the calculation of the effect of higher multipoles on the ground-state mass and for the calculation of fission-barrier heights. Because of these improvements, the 1981 calculation was sufficiently accurate to show P_3 (octupole) effects on masses near ^{222}Ra and P_6 effects on masses near ^{252}Fm. The observation of the octupole effects on nuclear masses provided the seed stimulus for a revived interest in the properties of nuclei near ^{222}Ra, as summarized in the extensive paper [41]) by Leander and Chen. The improved model also showed the presence of a peninsula of stability [17]) extending from the superheavy island towards the heaviest known elements.

In 1984 it was shown that the incorporation of the finite-range surface energy and an exponential term [18]) to the original droplet model [8–10]) resulted in dramatic improvements in its predictive properties, as summarized in the discussion of table A in ref. [19]). Mass calculations based on both the FRLDM [15]) and the FRDM [19]) were presented in the 1988 review of mass models in Atomic Data and Nuclear Data Tables. These calculations also used an improved pairing model relative to that used in the 1981 work. In the 1988 results the error in the FRDM was about 10% lower than that in the FRLDM.

There were two major unresolved issues in the 1988 calculations. First, there still existed some deficiencies in the pairing model and parameter choices that were used. Second, ϵ_3 and ϵ_6 shape degrees of freedom were still not included, so deviations between calculated and measured masses due to the omission of these shape degrees of freedom were still present. Extensive investigations of pairing models and their parameters have now been completed and resulted in an improved formulation of the pairing model [33]). We have now also minimized the potential energy with respect to ϵ_3 and ϵ_6 shape degrees of freedom. An overview of the results has been given in a paper on Coulomb redistribution effects [42]).

3.4. Recent mass model improvements

The FRDM, which includes Coulomb redistribution effects, is now the preferred nuclear mass model. Relative to the work described in refs. [42,43]) further improvements have been incorporated into the model. First, it was found that the γ zero-point energy could not be sufficiently

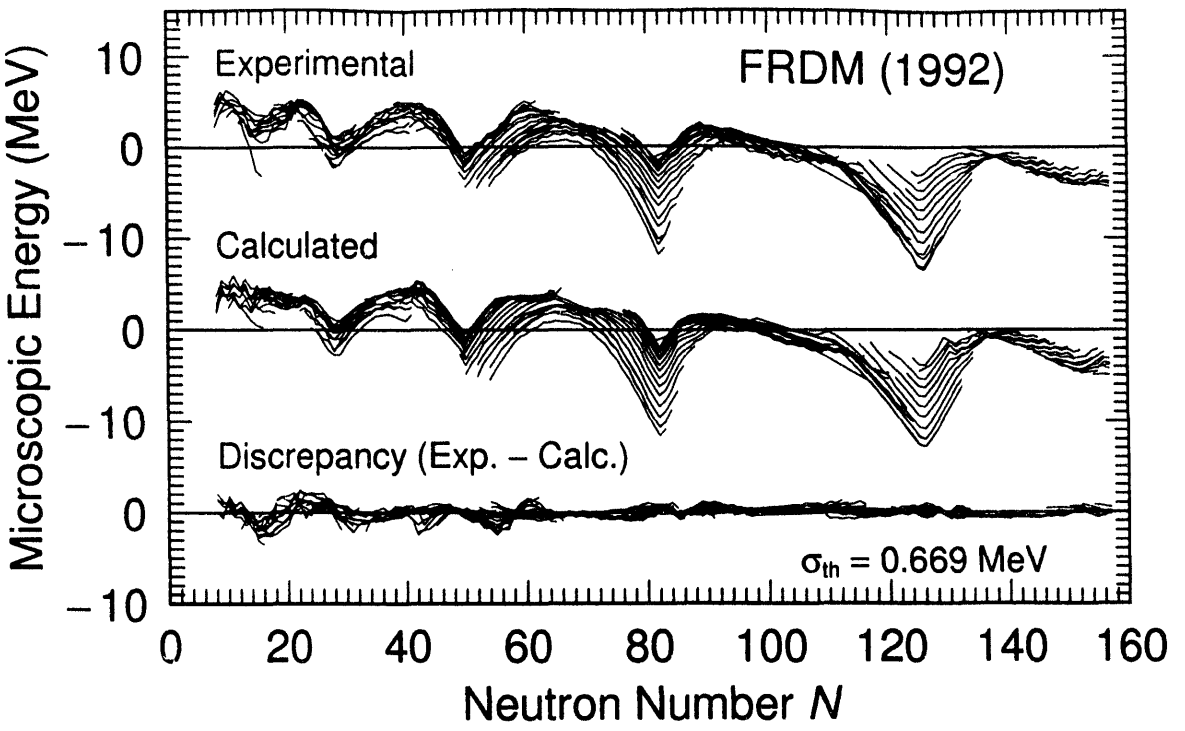

Figure 2. Comparison of experimental and calculated microscopic corrections for 1654 nuclei, for a macroscopic model corresponding to the finite-range droplet model. The bottom part showing the difference between these two quantities is equivalent to the difference between measured and calculated ground-state masses. There are almost no systematic errors remaining for nuclei above $N = 65$, for which region the theoretical error is only 0.448 MeV. The results shown in this figure represent our new mass model.

accurately calculated in our current model. It is therefore no longer included, whereas the ϵ zero-point energy is retained. Second, we have also returned to the original prescription of including basis functions corresponding to 12 oscillator shells for all A values, instead of using somewhat fewer basis functions for lighter nuclei[42,43]). Third, we now use an eighth-order Strutinsky shell correction with a range $\gamma = 1.0\,\hbar\omega$ instead of our earlier choice of a sixth-order Strutinsky shell correction with the same range. The change in zero-point energy reduced the error in the calculated neutron separation energies from 0.551 MeV to 0.444 MeV and the mass error from 0.778 MeV[42,43]) to 0.773 MeV. The second and third improvements further reduced the separation-energy error to 0.411 MeV and the mass-model error to 0.669 MeV.

Figure 2 shows the results of the FRDM calculation. As usual, the top part shows the differences between measured masses and the spherical macroscopic FRDM contribution plotted against the neutron number N, with isotopes of a particular element connected by a line. These "experimental microscopic corrections" are to be compared with the calculated microscopic corrections, which are plotted in the middle part of the figure. When the macroscopic and microscopic parts of the mass calculation are combined and subtracted from the measured masses the deviations in the bottom part of the figure remain. The trends of the error in the heavy region suggest that this mass model should be quite reliable for nuclei beyond the current end of the periodic system. When ϵ_3 and ϵ_6 shape degrees of freedom were included in the mass calculations it became clear that the FRLDM, which does not treat Coulomb redistribution effects, is deficient in the heavy-element region, as is seen in fig. 3.

Because the Coulomb redistribution term that is included in the FRDM is proportional to

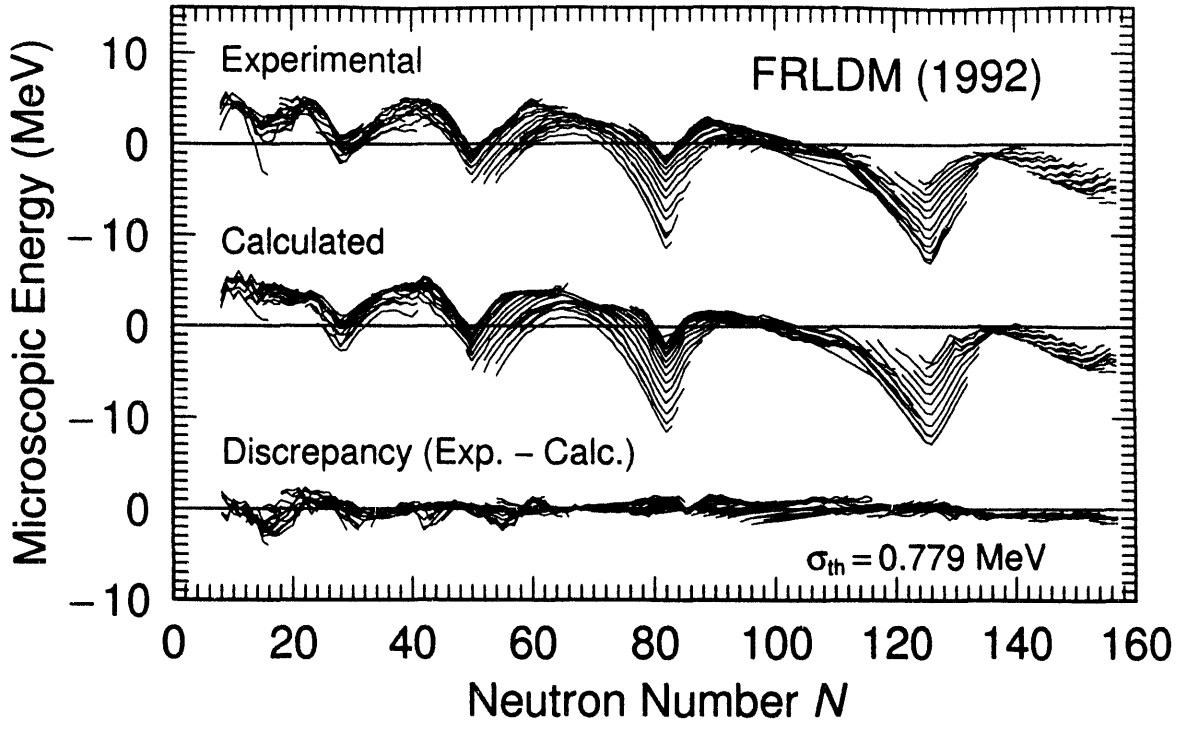

Figure 3. Analogous to fig. 2, but for the finite-range liquid-drop model, which contains no Coulomb redistribution terms. This leads to the systematic errors in the heavy region, where the negative errors indicate that calculated masses are systematically too high.

$Z^2A^{1/3}$ this term grows very rapidly for increasingly heavy nuclei. One therefore expects that masses calculated in models that do not account for Coulomb redistribution effects will diverge as one moves towards heavier nuclei. This is borne out by our calculations where we find, for example, a 3-MeV difference for $^{272}110$ between the FRDM prediction of 133.82 MeV and the FRLDM prediction of 136.61 MeV. Thus, according to the FRDM, in heavy-ion reactions the compound system is created at a higher excitation energy relative to predictions of models that do not account for Coulomb redistribution effects.

Finally, we compare in fig. 4 our results to those calculated with the ETFSI-1 model[44,45]). It is the only other recent global mass calculation based on a quantal treatment of the nucleon interaction that we are aware of. In the graph we show the difference between measured masses and calculated masses for the two models. For the FRDM we have limited the plot to $A \geq 36$, which is the region considered in the ETFSI-1 calculation. Because slightly different experimental data bases were used in the two investigations, the number of nuclei in the top and bottom parts of the figure are not the same. One observes that the FRDM has considerably smaller errors in the heavy region, and that the strong odd-even staggering present in the ETFSI-1 results is absent in the top curve.

3.5. Estimation of model errors

In most earlier studies[16,46]), the error of a theoretical mass model was taken to be the root-mean-square (rms) deviation

$$\sigma_{\rm rms} = \left[\frac{1}{n}\sum_{i=1}^{n}(M^i_{\rm exp} - M^i_{\rm th})^2\right]^{1/2} \qquad (1)$$

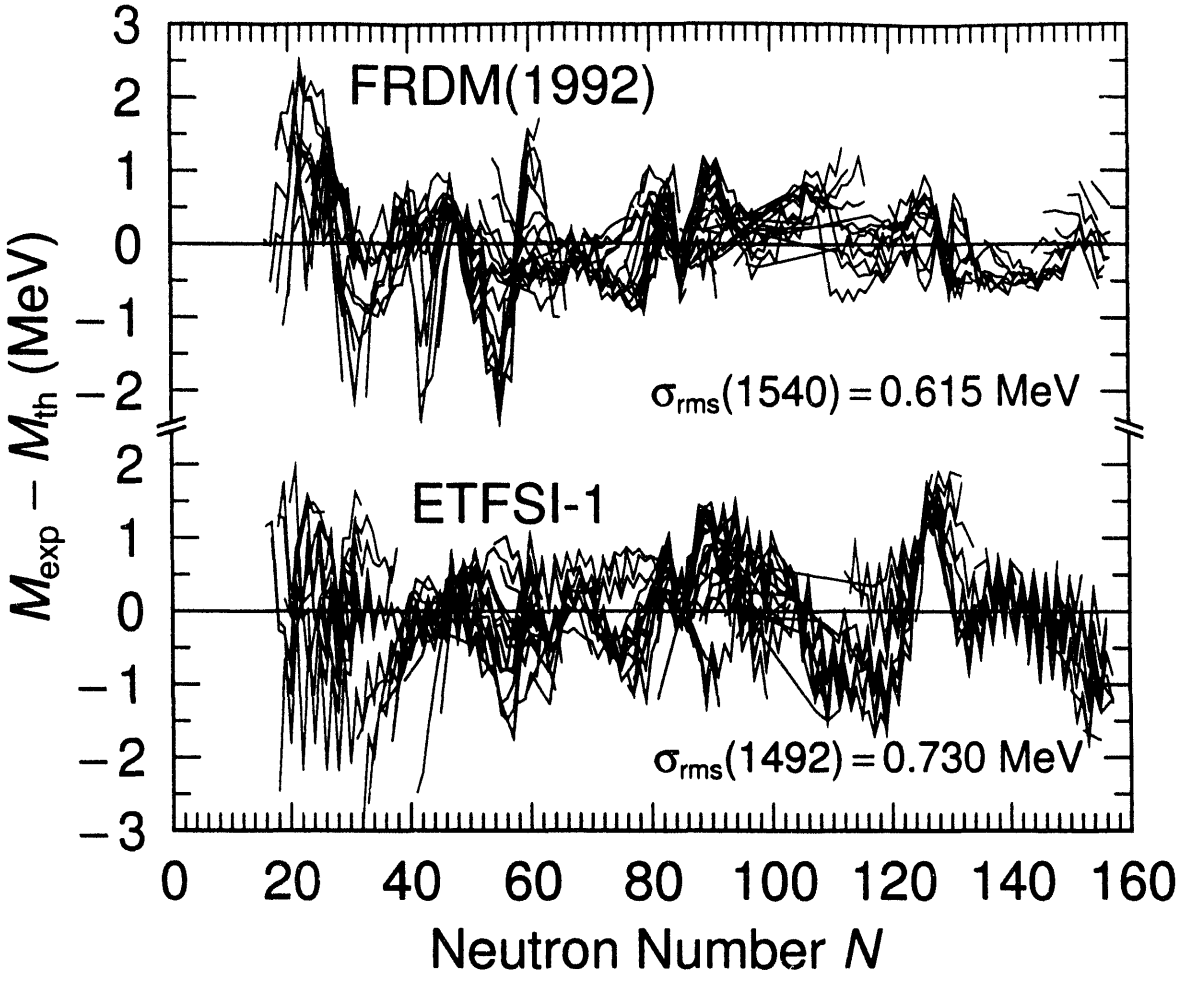

Figure 4. Comparison of discrepancies between measured and calculated masses for two models. The ETFSI-1 model shows a strong odd-even staggering, indicating a problem in the pairing model. The FRDM gives better agreement with experimental masses, especially in the heavy region.

and the parameters of the model were determined by minimizing $\sigma_{\rm rms}$ in eq. (1). Here $M^i_{\rm th}$ is the calculated mass and $M^i_{\rm exp}$ is the measured mass for a particular proton-neutron combination specified by Z and N. If one assumes that the calculated masses have a Gaussian distribution around the true mass with zero mean deviation and if the measured masses have zero error, then the maximum-likelihood estimate for the standard deviation of the Gaussian distribution of the model error is *exactly* $\sigma_{\rm rms}$. In the more general and realistic situation where the measured masses are associated with errors, eq. (1) is an incorrect estimator of model error since it will contain contributions from the experimental errors. It is reasonable to define model error as before, with the further assumption that the model error may have a non-zero mean deviation $\mu_{\rm th}$ from the experimental masses. With these definitions the equations that determine the model adjustable parameters p_ν and the error quantities $\sigma_{\rm th}$ and $\mu_{\rm th}$ are:

$$\sum_{i=1}^{i=n} \frac{[M^i_{\rm exp} - (M^i_{\rm th} + \mu_{\rm th}{}^*)]}{{\sigma^i_{\rm exp}}^2 + {\sigma_{\rm th}}^{2*}} \frac{\partial M^i_{\rm th}}{\partial p_\nu} = 0, \quad \nu = 1, 2, \ldots, m \tag{2}$$

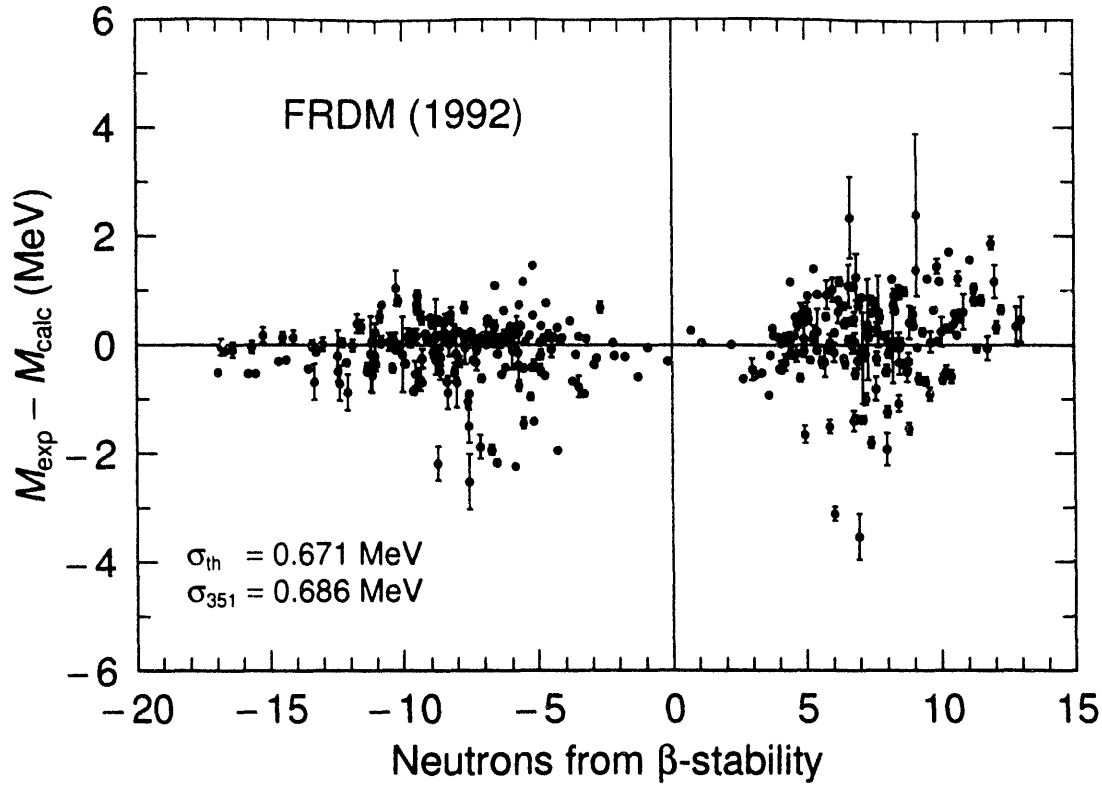

Figure 5. Calculation to show model reliability in new regions of nuclei. Here we used a smaller set of measured masses to adjust the model parameters than in the full calculation shown in fig. 2. The errors for nuclei not included in the adjustment are displayed in this figure. The error is only 2% larger than in the region to which the model parameters were adjusted. The larger deviations for two oxygen nuclei 6 and 7 neutrons from β-stability may indicate that light nuclei this close to the neutron drip line are outside the range of model applicability.

$$\sum_{i=1}^{i=n} \frac{[M^i_{exp} - (M^i_{th} + \mu_{th}{}^*)]^2 - ({\sigma^i_{exp}}^2 + {\sigma_{th}}^{2*})}{({\sigma^i_{exp}}^2 + {\sigma_{th}}^{2*})^2} = 0 \tag{3}$$

and

$$\sum_{i=1}^{i=n} \frac{[M^i_{exp} - (M^i_{th} + \mu_{th}{}^*)]}{({\sigma^i_{exp}}^2 + {\sigma_{th}}^{2*})} = 0 \tag{4}$$

A more complete discussion of our error analysis is presented in refs. [15,43]). To allow for a single error measure that is similar to an rms deviation between the data and model we also calculate the square root of the second central moment of the error term, $\sigma_{th;\mu=0}$. This quantity is obtained by setting $\mu_{th} = 0$ when solving eq. (3). In contrast to the rms measure, it has the advantage that it has no contributions from the experimental errors.

A common misconception is that one has to "throw away" data points that have errors that are equal to or larger than the error of the model whose parameters are determined. When the above formalism is used, this is no longer necessary.

3.6. Extrapability of nuclear mass models

One test of the reliability of a nuclear mass model is to compare deviations between measured and calculated masses in new regions of nuclei that were not considered when the model pa-

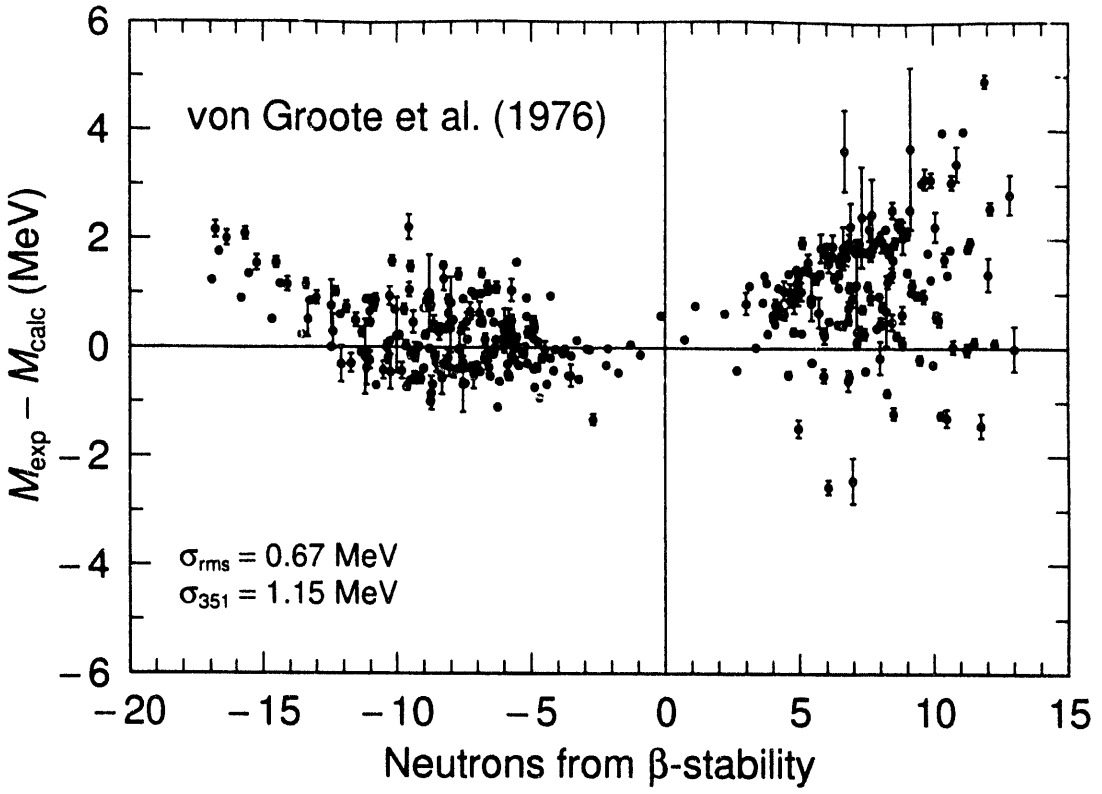

Figure 6. Analogous to fig. 5 but for the model of von Groote et al. [47]). For this model with postulated shell corrections and more adjustable parameters than our model with *calculated* shell corrections, the error grows by 72% in the new region relative to the error in the region where the parameters were adjusted. There is also a systematic increase in the error with increasing distance from β-stability.

rameters were determined to deviations in the original region. This type of analysis was used earlier by Haustein [46]). However, we here considerably modify his analysis. In addition to examining the raw differences between measured and calculated masses, we use these differences to determine the *model* mean discrepancy μ_{th} from the true masses and the *model* standard deviation σ_{th} around this mean. Whereas the raw differences do not show the true behavior of the theoretical error because errors in the measurements contribute to these differences, by use of the ideas developed in the previous section we are able to estimate the *true* mean and standard deviation of the theoretical error term e_{th}.

Since our new mass model was developed only recently, we cannot test its reliability in new regions of nuclei because sufficiently many new data points are not available. Therefore, we have resorted to a simple simulation, in which we adjusted the model parameters to the same experimental data set that was used in our 1981 mass calculation [16]). Consequently, this calculation is not quite identical to the one on which fig. 2 is based. The differences between the 351 new masses that are now measured [48]) and the calculated masses are plotted versus neutrons from β-stability in fig. 5. We note no systematic increase in the error with increasing neutrons from β-stability. For the new region of nuclei the square root of the second central moment is 0.686 MeV, compared to 0.671 MeV in the region where the parameters were adjusted, representing an increase of only 2%.

Mass models based on postulated shell-correction terms and a correspondingly larger number of parameters normally diverge outside the region where the parameters were determined. As an example of such behavior, we show in fig. 6 the error of the von Groote et al. [47])

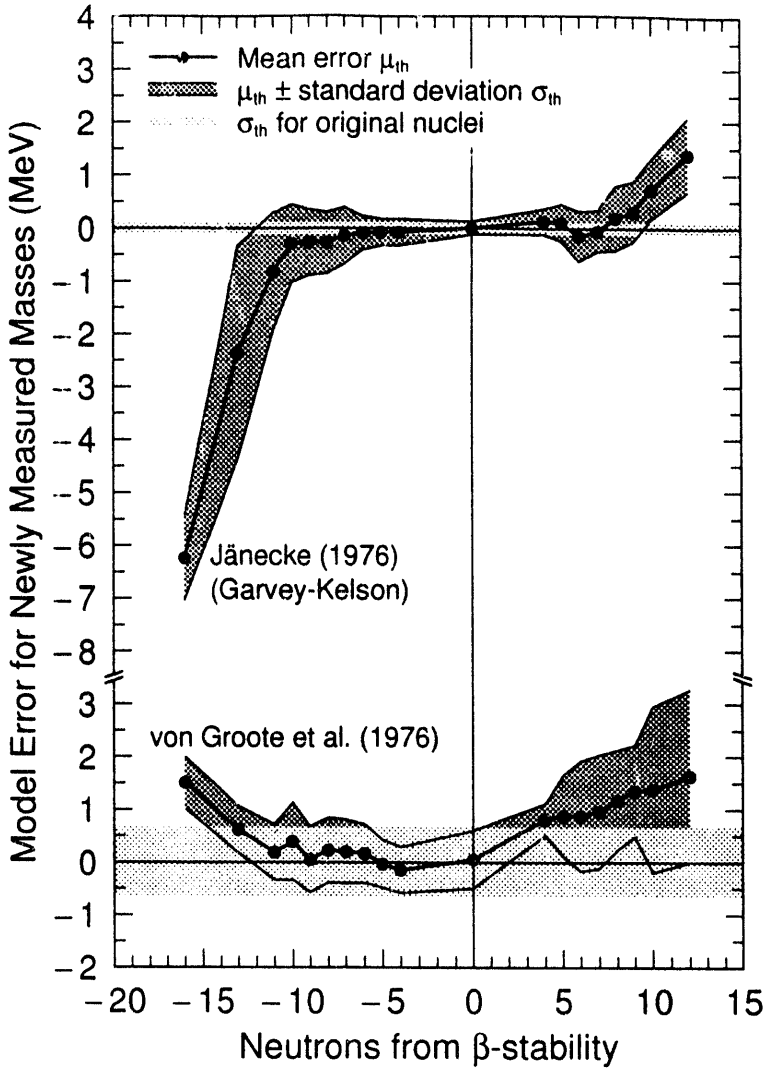

Figure 7. Comparison of error behavior for two models applied to new nuclei versus distance from β-stability. Compare this figure to fig. 8, which is plotted to the same scale.

mass calculation for the same region of nuclei.

To study more quantitatively how the error depends upon distance from β-stability, we introduce bins in the error plots sufficiently wide to contain about 10–20 points and calculate the mean error and standard deviation about the mean for each of these bins. The results for the two models shown in figs. 5 and 6 and for five other models are displayed in figs. 7 and 8. For each model the central, light-gray band representing the original error region extends one standard deviation on each side of zero. The solid dots connected by a thick black line represent the mean of the error for nuclei that were not considered when the model parameters were determined. The dark gray area extends one standard deviation on each side of this line. The properties of the seven models displayed in figs. 7 and 8, as well as those of a recent neural network calculation[49], are summarized in table 1.

In is of interest to note that for the three models that are based on a quantal treatment of the nuclear interactions, namely the three models in the lower part of fig. 8, *only two* of the points representing the mean deviation fall, just barely, outside the original error region. Also, the full error of the three models for new nuclei usually falls inside the error region corresponding to the original data set. Also, there are no systematic increases of the error

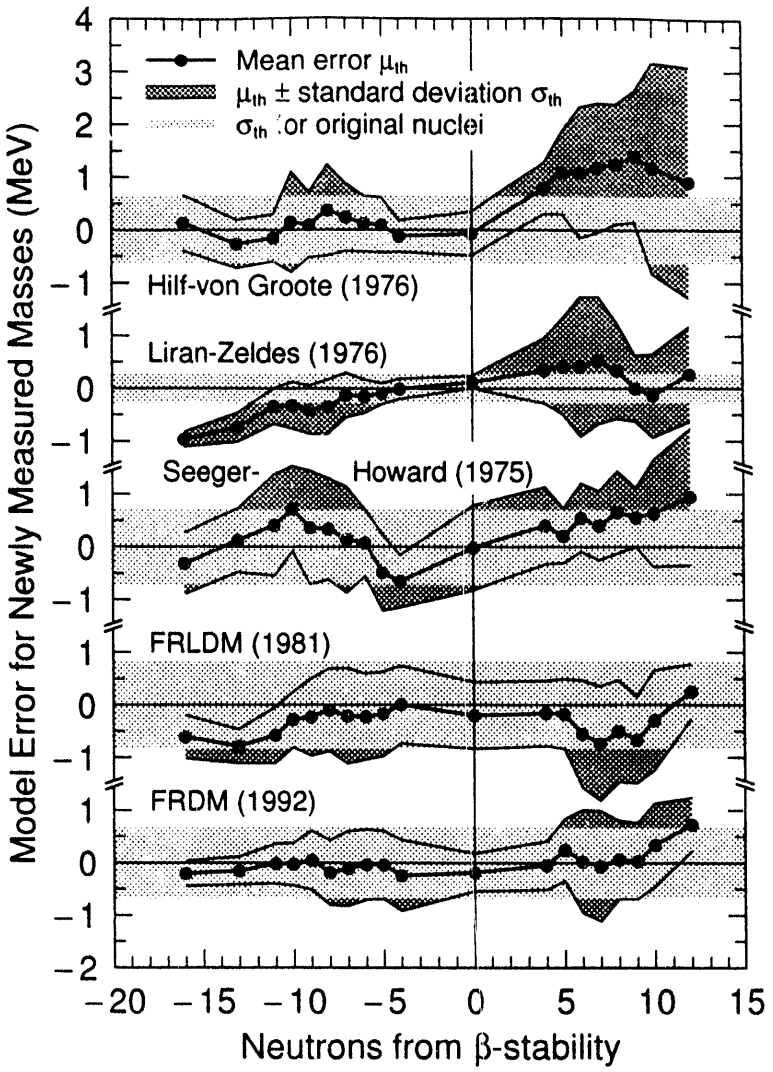

Figure 8. Comparison of error behavior for five mass models applied to new nuclei versus distance from β-stability. Compare this figure to fig. 7, which is plotted to the same scale.

with increasing distance from β-stability, with the possible exception of the Seeger-Howard model on the neutron-rich side. This model is based on a Nilsson modified-oscillator single-particle potential. The spin-orbit and pseudo-difuseness parameters of this potential vary rather dramatically over the periodic system, in contrast to the behavior of these parameters in the folded-Yukawa single-particle potential used in the FRLDM and FRDM calculations. Therefore, even though they are based on a quantal treatment of the nuclear interaction, the Seeger-Howard results may be less reliable for new regions of nuclei than calculations based on folded-Yukawa or Woods-Saxon potentials. In summary, we feel that at least the FRLDM and FRDM show substantial promise of being reliable as the proton and neutron drip lines are approached.

In contrast, it is clear that the remaining models that are not based on a quantal treatment of the nuclear interaction quickly diverge when applied to nuclei outside the region where their parameters were originally adjusted. One can expect that they would become even more unreliable when applied even further from stability.

Table 1. Comparison of errors of different mass calculations. The errors are tabulated both for the region in which the parameters were originally adjusted and for a set of new nuclei that were not taken into account in the determination of the parameters of the mass models. The error ratio is the ratio between the numbers in columns 9 and 3, except for the last line, where column 6 is used instead of column 9. It would have been preferable to use the error in column 4 instead of that in column 3, since $\sigma_{\rm th}$ does not contain contributions from the experimental errors. However, as can be seen in the table, the difference between the rms error and $\sigma_{\rm th}$ is small in the original region, where masses can be measured with smaller experimental errors than is possible far from β-stability.

		Original nuclei		New nuclei					
Model	$N_{\rm par}$	$\sigma_{\rm rms}$ (MeV)	$\sigma_{\rm th}$ (MeV)	$N_{\rm nuc}$	$\sigma_{\rm rms}$ (MeV)	$\mu_{\rm th}$ (MeV)	$\sigma_{\rm th}$ (MeV)	$\sigma_{{\rm th};\mu=0}$ (MeV)	Error ratio
J. (G.-K.)	~ 500	0.118		337	1.461	− 0.278	1.428	1.455	12.33
v. G. et al.	~ 50	0.67		351	1.193	0.612	0.978	1.154	1.72
H. et al.	~ 50	0.66		351	1.271	0.519	1.124	1.237	1.87
L.-Z.	178	0.276		346	0.912	− 0.044	0.736	0.738	2.67
S.-H.	9	0.704		309	0.976	0.289	0.910	0.956	1.36
FRLDM	9	0.835	0.831	351	0.911	− 0.321	0.826	0.884	1.06
FRDM	14	0.673	0.671	351	0.735	− 0.004	0.686	0.686	1.02
Neural net	421	0.828		351	5.981				7.22

3.7. Other properties of nuclear mass models

For some nuclear mass models, it has not been possible for us to study their behavior for new nuclei far from β-stability for several reasons. Some models have been developed only recently, so there is not yet sufficiently many new masses to make a statistically significant analysis. Others have been developed sufficiently long ago that new mass measurements are available, but the models were originally applied to such a limited region of nuclei that again a statistical analysis is not possible. However, for any model one may discuss how it fulfills the few standard requirements for a physical theory that were discussed in the introduction.

We have not been able to test the extrapability of the ETFSI-1 model but have investigated the differences between the FRDM and the ETFSI-1 model far from β-stability. Normally, the differences between the models are only an MeV or so, but close to the neutron drip lines the FRDM masses are about 3 MeV more bound in the region below Pb. Above Pb the situation is reversed and the FRDM masses may be 3 or more MeV less bound than the ETFSI-1 masses near the neutron drip line. In the neutron-deficient superheavy region the FRDM masses are more bound by 2–4 MeV relative to the ETFSI-1 masses.

4. Conclusions

Although mass models based on postulated microscopic corrections with a large number of adjustable parameters have small errors in the region where the parameters were adjusted, they diverge severely when applied outside this region. The error is typically larger by 100% or more in the new region than in the region where the model parameters were determined, and the errors in most cases grow with distance from β-stability. In contrast, models based on a quantal treatment of the nuclear interaction show remarkable stability when applied to new nuclei that were not considered when the models were initially formulated and their parameters determined.

Another tremendous advantage of the microscopic mass models is that their sound physical basis makes it possible to interpret discrepancies between calculated and experimental masses in terms of new physical effects. In our own work, this has allowed the identification of octupole effects on nuclear masses in the ^{222}Ra region, the discovery (in parallel but independently of experiments) of a deformed neutron-deficient superheavy region, and the discovery of Coulomb redistribution effects on nuclear masses.

From the developments in nuclear-structure models over the last several years and the application of these models to astrophysical calculations one can draw the following conclusions:

- Mass models based on postulated microscopic corrections and a large number of parameters are no longer worthwhile, and a disproportionate amount of effort on such models should be avoided. Instead, the focus should be to develop further the microscopic models that have provided so much insight into nuclear structure.

- Mass models based on calculated microscopic effects are now sufficiently reliable far from β-stability to contribute to the understanding of the r-process [50]).

- The macroscopic-microscopic approach, in particular the FRDM version, is now used for not only mass calculations, but also for the calculation of β-decay rates, delayed neutron emission probabilities, fission barriers, pairing gaps, spins of the ground-state and excited-state levels, and level densities, which are then used in various astrophysical studies.

- Our *unified* approach, based on actually calculating microscopic nuclear-structure effects in a single model by solving the Schrödinger equation, is now in some cases making it possible to identify characteristic features in astronomical data as clear nuclear-structure signatures or, alternatively, as stellar dynamical effects.

This work was supported by the U. S. Department of Energy and by the Japan Atomic Energy Research Institute.

References

1) V. M. Strutinsky, Nucl. Phys. **A95** (1967) 420.

2) V. M. Strutinsky, Nucl. Phys. **A122** (1968) 1.

3) S. G. Nilsson, C. F. Tsang, A. Sobiczewski, Z. Szymański, S. Wycech, C. Gustafson, I.-L. Lamm, P. Möller, and B. Nilsson, Nucl. Phys. **A131** (1969) 1.

4) M. Brack, J. Damgaard, A. S. Jensen, H. C. Pauli, V. M. Strutinsky, and C. Y. Wong, Rev. Mod. Phys. **44** (1972) 185.

5) M. Bolsterli, E. O. Fiset, J. R. Nix, and J. L. Norton, Phys. Rev. **C5** (1972) 1050.

6) W. D. Myers and W. J. Swiatecki, Nucl. Phys. **81** (1966) 1.

7) W. D. Myers and W. J. Swiatecki, Ark. Fys. **36** (1967) 343.

8) W. D. Myers and W. J. Swiatecki, Ann. Phys. (N. Y.) **55** (1969) 395.

9) W. D. Myers and W. J. Swiatecki, Ann. Phys. (N. Y.) **84** (1974) 186.

10) W. D. Myers, Droplet model of atomic nuclei (IFI/Plenum, New York, 1977).

11) W. D. Myers, Atomic Data Nucl. Data Tables **17** (1976) 411.

12) H. J. Krappe and J. R. Nix, Proc. Third IAEA Symp. on the physics and chemistry of fission, Rochester, 1973, vol. I (IAEA, Vienna, 1974) p. 159.

13) H. J. Krappe, J. R. Nix, and A. J. Sierk, Phys. Rev. **C20** (1979) 992.

14) J. Blocki, J. Randrup, W. J. Swiatecki, and C. F. Tsang, Ann. Phys. (N. Y.) **105** (1977) 427.

15) P. Möller and J. R. Nix, Atomic Data Nucl. Data Tables **39** (1988) 213.

16) P. Möller and J. R. Nix, Nucl. Phys. **A361** (1981) 117.

17) P. Möller and J. R. Nix, Atomic Data Nucl. Data Tables **26** (1981) 165.

18) P. Möller, W. D. Myers, W. J. Swiatecki, and J. Treiner, Proc. 7th Int. Conf. on nuclear masses and fundamental constants, Darmstadt-Seeheim, 1984 (Lehrdruckerei, Darmstadt, 1984) p. 457.

19) P. Möller, W. D. Myers, W. J. Swiatecki, and J. Treiner, Atomic Data Nucl. Data Tables **39** (1988) 225.

20) J. R. Nix, Ann. Rev. Nucl. Sci. **22** (1972) 65.

21) P. Möller and J. R. Nix, Proc. Third IAEA Symp. on the physics and chemistry of fission. Rochester, 1973, vol. I (IAEA, Vienna, 1974) p. 103.

22) P. Möller, S. G. Nilsson, and J. R. Nix, Nucl. Phys. **A229** (1974) 292.

23) J. Dudek, Z. Szymański, T. Werner, A. Faessler, and C. Lima, Phys. Rev. **C26** (1982) 1712.

24) U. Mosel and H. W. Schmitt, Phys. Rev. **C4** (1971) 2185.

25) Å. Bohr, B. R. Mottelson, and D. Pines, Phys. Rev. **110** (1958) 936.

26) S. T. Belyaev, Kgl. Danske Videnskab. Selskab. Mat.-Fys. Medd. **31**:No. 11 (1959).

27) S. G. Nilsson and O. Prior, Kgl. Danske Videnskab. Selskab. Mat.-Fys. Medd. **32**:No. 16 (1961).

28) W. Ogle, S. Wahlborn, R. Piepenbring, and S. Fredriksson, Rev. Mod. Phys. **43** (1971) 424.

29) P. Möller, J. R. Nix, W. D. Myers, and W. J. Swiatecki, Atomic Data Nucl. Data Tables (1993) to be published.

30) H. J. Lipkin, Ann. Phys. (N. Y.) **9** (1960) 272.

31) Y. Nogami, Phys. Rev. **134** (1964) B313.

32) H. C. Pradhan, Y. Nogami, and J. Law, Nucl. Phys. **A201** (1973) 357.

33) P. Möller and J. R. Nix, Nucl. Phys. **A536** (1992) 20.

34) I. Hamamoto, Nucl. Phys. **62** (1965) 49.

35) J. A. Halbleib, Sr. and R. A. Sorensen, Nucl. Phys. **A98** (1967) 542.

36) J. Randrup, C. F. Tsang, P. Möller, S. G. Nilsson, and S. E. Larsson, Nucl. Phys. **A217** (1973) 221.

37) J. Krumlinde and P. Möller, Nucl. Phys. **A417** (1984) 419.

38) P. Möller and J. Randrup, Nucl. Phys. **A514** (1990) 1.

39) P. Möller and J. R. Nix, Nucl. Phys. **A272** (1976) 502.

40) P. Möller, J. R. Nix, and W. J. Swiatecki, Nucl. Phys. **A492** (1989) 349.

41) G. A. Leander and Y. S. Chen, Phys. Rev. **C37** (1988) 2744.

42) P. Möller, J. R. Nix, W. D. Myers, and W. J. Swiatecki, Nucl. Phys. **A536** (1992) 61.

43) P. Möller and J. R. Nix, Proc. 6th Int. Conf. on nuclei far from stability and 9th Int. Conf. on nuclear masses and fundamental constants, Bernkastel-Kues, 1992 (IOP Publishing, Bristol, 1993) p. 43.

44) J. M. Pearson, Y. A. Aboussir, A. K. Dutta, R. C. Navak, M. Farine, and F. Tondeur, Nucl. Phys. **A528** (1991) 1.

45) Y. Aboussir, J. M. Pearson, A. K. Dutta, and F. Tondeur, Nucl. Phys. **A549** (1992) 155.

46) P. E. Haustein, Proc. 7th Int. Conf. on nuclear masses and fundamental constants, Darmstadt-Seeheim, 1984 (Lehrdruckerei, Darmstadt, 1984) p. 413.

47) H. von Groote, E. R. Hilf, and K. Takahashi, Atomic Data Nucl. Data Tables **17** (1976) 418.

48) G. Audi, Midstream atomic mass evaluation, private communication (1989), with four revisions.

49) K. A. Gernoth, J. W. Clark, J. S. Prater, and H. Bohr (1992) to be published.

50) K.-L. Kratz, J.-P. Bitouzet, F.-K. Thielemann, P. Möller, and B. Pfeiffer, Ap. J. **403** (1993) 216.

END

DATE
FILMED
3/15/94